Article

Tuning a Colloidal Synthesis to Control Co Doping in Ferrite Nanocrystals

Gabriel Shemer, Einat Tirosh, Tsachi Livneh, and Gil Markovich

J. Phys. Chem. C, **2007**, 111 (39), 14334-14338 • DOI: 10.1021/jp0736793

Tuning a Colloidal Synthesis to Control Co^{2+} Doping in Ferrite Nanocrystals

Gabriel Shemer,[†] Einat Tirosh,[†] Tsachi Livneh,[‡] and Gil Markovich*,[†]

School of Chemistry, Raymond and Beverly Sackler Faculty of Exact Sciences, Tel-Aviv University, Tel Aviv 69978, Israel, and Department of Physics, Nuclear Research Center, Negev, P.O. Box 9001, Beer-Sheva, 84190 Israel

Received: May 14, 2007; In Final Form: July 4, 2007

Cobalt−ferrite nanocrystals were synthesized using a high-temperature organometallic decomposition scheme in the presence of surfactant molecules. The influence of the addition of cosurfactant molecules of polyol type on the resulting nanocrystals was examined. The properties of the nanocrystals were studied using electron microscopy, and magneto-optical and Raman spectroscopies. The addition of the cosurfactants was found to influence the growth mechanism of the nanocrystals, resulting in a significant reduction in the concentration of the Co^{2+} ions incorporated into the ferrite lattice up to a factor of 4 and an increase in the size of the synthesized nanocrystals. In addition, control over the occupation of octahedral versus tetrahedral coordination sites by the cobalt ions was demonstrated.

Introduction

The synthesis of well-separated, organically capped nanocrystals in solution provides a controllable building block that can be used for the formation of various nanostructures, such as ordered arrays of various dimensions[1,2] and nanoscale functional devices.[3,4] Such nanocrystals are usually prepared by wet colloidal synthesis techniques, which are limited to maximal temperatures of 300−350 °C by the organic solvents used. This is in contrast to bulk metal oxide preparations, for example, where much higher annealing temperatures are typically required to obtain well-crystalline, stoichiometrically precise materials.[5] Thus, in the case of colloidal metal oxide nanocrystals, special low-temperature methods are required to produce monodisperse metal oxide nanocrystals of the desired crystal structure and composition. These properties are strongly dependent on the synthesis condition, for example, the solvents and surfactants used,[6] the applied temperature and pressure,[7] the duration of the synthesis, and the concentration of the precursors.[8]

In a case where magnetite (Fe_3O_4) nanoparticles were synthesized from organometallic precursors using heptadecanoic acid, a strong Lewis acid stabilizing agent, it was demonstrated that this acid slows the growth processes during the ripening thus reducing the formation of interfacial defects.[9] Relatively small changes in the composition of synthesized nanoparticles may have an appreciable effect on their properties. In the case of blue-emitting $Zn_xCd_{1-x}Se$ nanocrystals, it was found that the size of the nanocrystals changed with the increased doping of zinc, thereby changing the photoluminescence properties.[10] Doping diamagnetic ZnO with manganese ions induced ferromagnetism in this material, both in bulk form[11] and in nanocrystals.[12] Another important example of a structure/composition-sensitive nanocrystalline magnetic compound is the case of FePt and its ordering in the highly magnetically anisotropic $L1_0$ phase.[13,14] $CoPt_3$ nanocrystals were synthesized by Weller and co-workers[15] that have shown that the synthesis kinetics was driven by the ratio between the rates of nucleation and growth, both largely responsible for the particle size.

Among colloidal metal oxide nanocrystals, the family of ferromagnetic oxides has been extensively studied. One particular example is cobalt−ferrite, which has been considered for high-density magnetic storage due to its large magnetic anisotropy.[16] In addition, it may be suitable for magneto-optical (MO) data storage as a result of its large MO coefficients.[17,18] Ferrites have a spinel type crystal structure,[19] where the lattice is constructed of a face-centered cubic structure of the oxygen ions and two types of metal cation interstitial sites, the tetrahedrally coordinated "A" site and the octahedrally coordinated "B" site. Cobalt−ferrite has a partially inverse spinel structure, where the Co^{2+} ions occupy both the A and B sites as does the Fe^{3+}. Many methods for the production of cobalt-doped ferrite nanocrystals were published in recent years,[20] including mechanical milling,[21] hydrothermal coprecipitation,[22] coprecipitation in a hydroxide solution,[23] microemulsion method,[24,25] sol−gel-like synthesis,[26] and coprecipitation in a microwave heating system.[27] The properties of the resultant nanoparticles depended on the conditions, precursors, and solvents with which they were produced.

In a previous article, a new method for synthesizing $CoFe_2O_4$ nanoparticles, using mixed metal precursors, was presented and compared to other published synthesis techniques.[28] MO spectroscopy was used to probe the cation distribution of cobalt ions within cobalt−ferrite nanoparticles. It was found that this synthesis scheme produced cobalt−ferrite nanoparticles with the most intense MO signal, reflecting the highest level of incorporation of Co^{2+} into the ferrite lattice. This level was higher by a factor of 2−3 than the other commonly used procedures. Standard characterization techniques (e.g., X-ray diffraction, magnetic measurements, and elemental analysis) could not detect differences between the various preparation techniques.

In this paper, we report on further development of the $CoFe_2O_4$ nanocrystals synthesis where by modifying one synthesis procedure the level of Co^{2+} incorporation in the nanocrystals was controlled. The synthesis developed by Sun et al.[29] was modified by using various cosurfactants and different

* To whom correspondence should be addressed.
[†] Tel-Aviv University.
[‡] Nuclear Research Center.

10.1021/jp0736793 CCC: $37.00
Published on Web 09/12/2007

TABLE 1: Description of the Precursors and Cosurfactants Used at Each Synthesis and the Average Size of the Produced Nanocrystals

sample	precursors	cosurfactant	size [nm]
I	iron(III)acac, Co(III)acac	1,2-hexadecanediol	9.1 ± 1.7
II	iron(III)acac, Co(II)acac	tetra ethylene glycol	6.5 ± 0.9
III	iron(III)acac, Co(III)acac	tetra ethylene glycol	5.9 ± 0.9
IV	iron(III)acac, Co(II)acac	1,2-hexadecanediol	8.6 ± 2.5
V	iron(III)acac, Co(II)acac		5.5 ± 1.1
VI	iron(III)acac, Co(II)acac, Zn(II)acac		5.0 ± 1.5

cobalt precursor valences. The use of a cosurfactant (or the lack of it) influenced the amount of cobalt inserted into the ferrite nanocrystal lattice. This was studied using two spectroscopic probes: MO spectroscopy determined the relative concentration of cobalt cations in the spinel interstices for the six different synthesis variants and Raman spectroscopy provided a sensitive tool to study the distribution of cobalt ions between octahedral and tetrahedral sites in the ferrite nanocrystals.

Experimental Methods

Synthesis. The six different syntheses of cobalt−ferrite nanoparticles, as summarized in Table 1, were performed under the same conditions. Each synthesis employed a different cosurfactant (apart from synthesis V, without a cosurfactant) and different valences of the cobalt precursor. In each synthesis, a total of 3 mmol of the metal precursors with 2:1 Fe/Co ratio (iron(III) acetylacetonate (Alfa Aesar), cobalt(II)/(III) acetylacetonate (Aldrich)), 6 mmol of each surfactant (oleic acid (Alfa Aesar) and oleylamine (Aldrich)), and 10 mmol of the cosurfactant (if used) (either 1,2-hexadecanediol or tetraethylene glycol) were added to 20 mL of benzyl ether (Aldrich) and stirred vigorously. Each synthesis was heated to 300 °C for 1 h under a nitrogen flow. Zinc(II) acetylacetonate (0.3 mmol) (Alfa Aesar) was added to the organometallic precursors without the presence of a cosurfactant (sample VI) to form zinc-doped cobalt−ferrite nanocrystals.

The resulting nanocrystals were precipitated by centrifugation at 6000 rpm for 5 min. The precipitate was dissolved in heptane, and then a mixture of acetone and ethanol was added to the solution followed by centrifugation and redispersion in heptane to obtain a purified nanocrystal solution.

Characterization. A Tecnai F20 transmission electron microscope (TEM) was used to obtain the size and the elemental analysis by energy dispersive X-ray spectroscopy (EDS) of the nanoparticles. Cobalt-ferrite nanoparticles were deposited from a heptane solution onto carbon grids for TEM.

Backscattering geometry Raman measurements were obtained from a Renishaw dispersive spectrometer by using an objective of $\times 50$ (NA = 0.8) at an excitation energy of 1.96 eV. The power density on the sample was kept low at $\sim 10^2$ W/cm^2 to avoid the damage of the samples.

The determination of the cation distribution in the cobalt−ferrite lattice was performed by measuring the magnetic circular dichroism (MCD) spectrum. MO spectroscopy is a well-established technique for the characterization of the electronic transitions in magnetic materials. The measurement system was described previously.[28] In short, a light modulation technique[30,31] was employed to measure the difference in the absorption coefficients between left- and right-circulalrly polarized light under the influence of an external magnetic field. The spectroscopic appartus consisted of a monochromated light source followed by a linear polarizer and a Hinds photoeleastic modulater. The polarized light was then passed through the poles of an electromagnet and transmitted through the samples. The outcoming signal was detected by a photomultiplier and separated into an AC and DC signals. The AC signal was lock-in amplified at the modulation frequency. Normalization of the MCD signal was performed by dividing the AC output by the DC. The cobalt−ferrite nanoparticle solutions were drop-casted onto clean quartz slides, and all the samples were measured under the same conditions. The normalized MCD signal was divided by the absorbance of the samples to obtain thickness independent MCD data.

Results

Figure 1 displays the TEM images of the cobalt−ferrite nanoparticles produced by the various syntheses. It can be seen that all syntheses produced roughly spherical nanoparticles with narrow size distributions, as shown in Table 1. EDS elemental analysis performed on approximately 100 particles from each synthesis revealed that the resultant nanocrystals contained the 1:2 ratio of cobalt to iron close to the initial ratio of the organometallic precursor molecules (see also ref 28), and in the case of the zinc-doped sample the metal atom percentage of the zinc was approximately 5%. As previously published, it was found that X-ray diffraction and magnetic measurements were not able to detect significant differences between different cobalt−ferrite preparations.[28]

The MCD spectra of the samples are shown in Figure 2. The peaks in the spectra represent electronic transitions of the Co^{2+} within the crystal. A broad band around 2.25 eV represents an intervalence charge transfer (IVCT) between the Co^{2+} and the Fe^{3+} ions in the octahedral interstices, and the band peak at 1.82 eV represents a crystal field transition at the cobalt ions in the tetrahedral interstices.[32] It can be clearly seen that sample V exhibited the most intense (negative) peaks in comparison to all other samples. The intensities of the MCD lines in Figure 2, which were normalized to the total Co^{2+} absorption of the samples, were proportional to the relative abundance of Co^{2+} ions at the corresponding sites. Samples II and III exhibited peaks with reduced intensities, and samples I and IV displayed the weakest MCD spectra. When a Co(III) precursor (for samples I and III) replaced the divalent cobalt precursor, the intensity of the IVCT band slightly increased relative to the case of a divalent precursor and the charge-transfer band corresponding to the tetrahedral sites slightly decreased. The doping of the cobalt−ferrite nanocrystals with zinc ions (sample VI) caused a reduction in the intensity of the peak at 1.82 eV, whereas the peak at 2.25 eV was intensified in comparison to sample V.

To better understand the differences between the various preparations samples IV and V were compared using Raman spectroscopy. These particular samples exhibited the largest differences in the MCD spectra as well as in the synthesis conditions (with and without the diol). Figure 3A,B displays Raman spectra of samples V and IV, respectively. Figure 3C shows the spectrum from the same exact spot where Figure 3A was taken after a five-fold increase in the He−Ne laser power. Four Raman lines around 474, 560, 615, and 682 cm^{-1} were identified in all three spectra. One difference between the spectra of samples IV and V is the intensity ratio between the major peaks at 474 and 682 cm^{-1}. Another difference is the appearance of a band around 645 cm^{-1} in sample V, which did not appear in sample IV. Upon laser heating, this band has practically disappeared, and the relative intensity of the 474 cm^{-1} band was increased. Nanocrystal heating is expected as a result of the high-optical absorption of the visible laser light by the

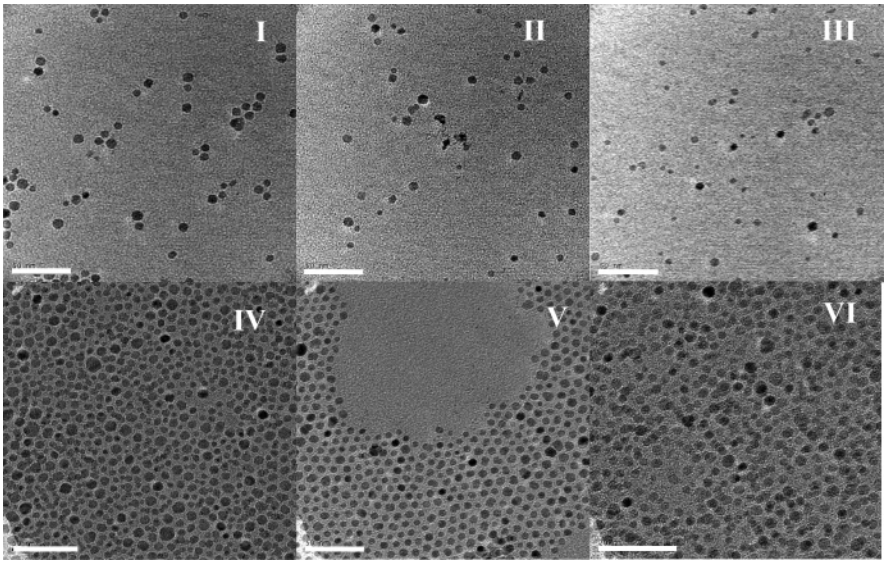

Figure 1. TEM images of the cobalt−ferrite nanoparticles synthesized using methods I−VI. The bar sizes are all 50 nm.

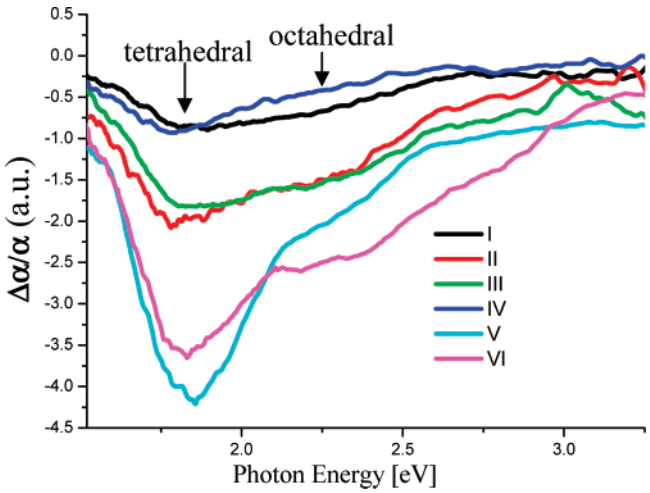

Figure 2. MCD spectra of the cobalt−ferrite nanocrystals prepared via syntheses I−VI. The arrows mark the assignment of the CD lines to octahedrally and tetrahedrally coordinated Co^{2+} according to ref 32.

cobalt−ferrite nanoparticles. Apart from annealing, which may be accompanied by structural relaxation and ion migration, heating may cause oxidation and degradation of the nanostructures. It was therefore beneficial to measure the sample temperature and to make sure that in our measurement the temperature did not go higher than ∼500 K, where Fe_3O_4 (and perhaps also $Co_xFe_{3-x}O_4$) oxidizes to γ-Fe_2O_3 first, followed by a transition to the α-Fe_2O_3 phase.[33]

The complete anti-Stokes and Stokes spectrum for sample IV is shown in Figure 4. For clarity the Stokes and anti-Stokes spectrum is shown after division by $(E_L - E_{ph})^4(n+1)$ and $(E_L + E_{ph})^4 n$, respectively, where the Bose factor is $n = (e^{(E_{ph}/kT)} - 1)^{-1}$, E_L is the incident laser energy, and E_{ph} is the phonon energy. This procedure allows changing T until the two spectra are similar in their intensities.[34] The estimation of the local temperature (with power density of $\sim 10^2$ W/cm^2) was performed by employing this procedure to the 474 cm^{-1} band and was calculated to be ∼355K for sample IV. A similar procedure for sample V gave $T \approx 430$ K. In both cases, T was far below the ∼500 K needed for the $Fe_3O_4 \rightarrow \gamma$-$Fe_3O_2$ phase transition. Increasing the power significantly resulted in oxidation into α-Fe_3O_2 (hematite).

Discussion

Sun and co-workers[29] have devised a nonhydrolytic synthetic scheme using organometallic precursors to obtain monodisperse ferrite nanoparticles (as in sample IV). They employed a long chain dialcohol to improve the nucleation of the ferrite nanoparticles. The use of a diol was reiterated by Zhang and coworkers,[35] where the long-chain diol was believed to mediate the availability of the cations for deposition and therefore assist in the crystallization of the cobalt−ferrite nanoparticles. In the present work, it was clearly observed that the presence of the cosurfactant significantly reduced the amount of Co^{2+} ions incorporated in the ferrite lattice. When the polyol cosurfactant molecules were completely removed from the synthesis (sample V), the MCD has markedly increased by a factor of ∼4 relative to sample IV.

In addition to the amount of cobalt ions inserted in the ferrite lattice, the size of the nanoparticles was also strongly influenced by the use of a cosurfactant (see Table 1). Thus, the presence of the polyol type cosurfactant had a direct influence on the growth mechanism of the nanoparticles. This mechanism may involve replacement of part of the acetylacetonate ligands with the diol molecules to form metal alkoxide molecules. The exchange of the acetylacetonate for the diol is probably facilitated by the elevated temperature and the presence of the oleic acid as a proton donor. The metal alkoxides may then react with other metal acetylacetonate molecules to form −M−O−M− (M = Fe or Co) by an ester elimination process.[36] In the absence of the diol, other −M−O−M− formation mechanisms are possible, for example, nonhydrolitic ether-like elimination, which is well known in nonaqueous sol−gel processes.[36] The diol-induced ester elimination growth mechanism may be faster than the other "thermal decomposition" mechanisms, which may lead to faster, cobalt-deficient growth.

The cobalt-deficient particle growth may be explained by the reduction potential of the diol. In a similar magnetite synthesis, it was postulated that under the same synthesis conditions the trivalent iron is partially reduced to divalent iron.[29] This may compete with the divalent cobalt in the non-hydrolytic growth process and would possibly lead to faster iron ion deposition due to differences in the energetics or rate constants involving the Co(II) reactions compared to the Fe(II) reactions. In addition, slow reduction of Co^{2+} to metallic Co by the diol during ferrite nanoparticle growth[37] could cause the accumulation of some

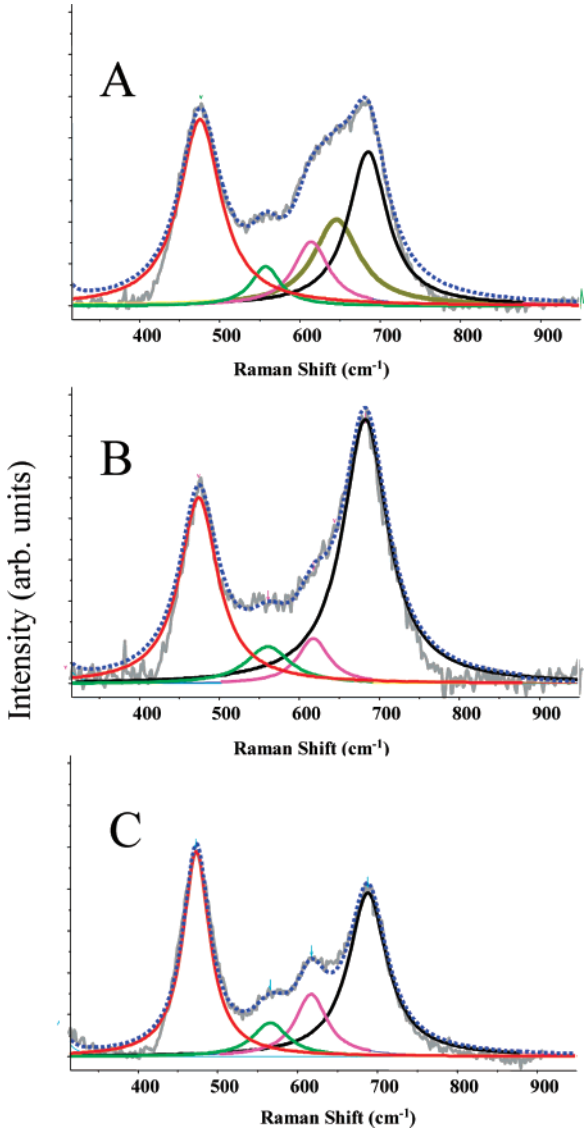

Figure 3. Raman spectra from sample V (A) and sample IV (B) taken at low-laser power of $\sim 10^2$ W/cm^2. (C) A spectrum from the exact spot where spectrum A was taken but after a 5-fold increase in the He−Ne laser power.

metallic Co clusters on the surface of the nanoparticles and subsequent oxidation to cobalt oxide impurity phase.

It is also known that diols are capable of coordinating to transition metal cations at iron oxide surfaces.[38] Being at a relatively high concentration, these molecules may compete with the oleic acid that probably binds stronger to the iron oxide surface and thus controls the final size of the growing particles.

In two of the syntheses, the valence of the cobalt precursor was changed to 3+ (samples I, III). In these cases, the MCD spectrum showed increased occupation of the octahedral sites relative to the syntheses where the divalent cobalt precursor was used. Nonmagnetic ions have been inserted into the spinel structure of ferrites to examine changes in the MO transitions.[39] Al^{3+} ions were inserted into ferrite crystals and were found to mainly occupy the octahedral sites. Because the ionic radii of Al^{3+} and Co^{3+} are similar when they are located in octahedral coordination,[40] Co^{3+} ions may preferentially occupy the octahedral sites, as observed experimentally. The deposited Co^{3+} may be reduced to Co^{2+} directly by the cosurfactant molecules or indirectly by octahedral Fe^{2+} ions that are likely to form due to the cosurfactant's reducing power. Contrary to aluminum, zinc ions predominantly occupy the tetrahedral sites when they

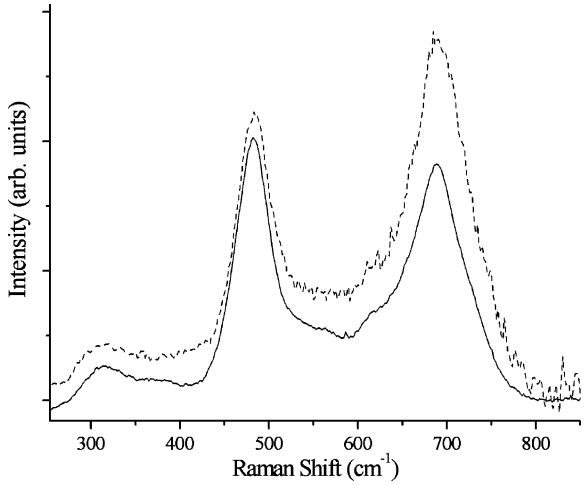

Figure 4. The Stokes (solid line) and anti-Stokes (dashed line) spectra for sample IV after division by $(E_L - E_{ph})^4(n + 1)$ and $(E_L + E_{ph})^4 n$, respectively.

are inserted into ferrites.[41] As seen in Figure 2, for sample VI, which is essentially sample V doped with Zn^{2+}, the MCD band corresponding to the Co^{2+} at tetrahedral sites was reduced due to occupation of these sites by Zn^{2+}. On the other hand, the MCD band corresponding to Co^{2+} at the octahedral sites was markedly increased, as expected.

Additional information about the coordination of the metal ions in the nanocrystals was obtained from the Raman spectroscopy. Cobalt−ferrite, like magnetite, has the inverse spinel structure with a cubic O_h^7 ($Fd\bar{3}m$) symmetry, giving rise to five Raman active modes, $3T_{2g} + E_g + A_{1g}$, with a large variability in the details of spectra measured on different samples.[42] More recently, a distorted, tetragonal structure was observed for bulk $CoFe_2O_4$ with 6 Raman active bands identified out of the 10 modes expected.[43] The Raman lines measured in this work are generally similar to those observed in previous publications. The low-frequency vibrations (below 600 cm^{-1}) are attributed to motion of oxygen around the octahedral lattice sites whereas the higher frequencies are attributed to oxygen around tetrahedral sites.[44] Thus, the intense band in the Raman spectra of the two samples at 682 cm^{-1} can be assigned to the A_{1g} symmetry (tetrahedral),[45] and the 474 cm^{-1} band is characteristic of the octahedral site.[44]

The Raman spectrum of magnetite has been extensively studied.[46] It has been found that magnetite has an intense peak at 670 cm^{-1}, which is attributed to the tetrahedral sites,[33] but no lines are detected around 470 cm^{-1}. Hence, the line at 682 cm^{-1} may consist of contributions of both the magnetite and cobalt−ferrite phases in the nanoparticles, and the band at 474 cm^{-1} is solely due to Co^{2+} at octahedral sites.

The difference in the intensity ratio of the two major Raman peaks at 682 and 474 cm^{-1} between sample V and IV conforms to the picture of higher Co^{2+} incorporation in sample V. The 682 cm^{-1} peak of sample IV is relatively large compared to the octahedral peak's intensity, while in sample V it is weaker. The MCD spectra show roughly similar tetrahedral to octahedral peak ratios for both samples. Thus, it is suggested that in the 682 cm^{-1} band of sample IV there is a large contribution of magnetite, or tetrahedrally coordinated iron ions to the Raman intensity, while in sample V this contribution is lower, that is, the contribution of the cobalt ions to the 682 cm^{-1} band in this sample is larger. This is particularly pronounced in the annealed sample V (Figure 3C).

The broad band around 645 cm^{-1} appearing in the Raman spectrum of sample V was not observed in bulk cobalt−ferrite

and is attributed to cobalt ions residing at defect sites that are probably located near the surface of the nanoparticles. This peak is particularly pronounced for sample V due to the higher surface-to-volume ratio of the nanoparticles in this sample. Upon laser heating sample V, these surface defects were annealed and a higher level of octahedral site occupation was observed (Figure 3C).

A noteworthy result is that the 682 cm^{-1} band was enhanced by ~30% in the anti-Stokes spectrum relative to the 474 cm^{-1} band (see Figure 4). The former band corresponds to the motion of oxygen around tetrahedral sites that are occupied by Co^{+2} and Fe^{+3}, and the latter corresponds to oxygen around octahedral sites. The observed asymmetry in the phonon intensity for the anti-Stokes and Stokes spectra probably comes about as a result of differing resonance conditions between the two sites for incident and scattered photons with the material's electronic transitions.

Conclusions

The details of a modification in a cobalt−ferrite colloidal nanocrystal synthesis were investigated using MO and Raman spectroscopy probes. The polyol cosurfactants were found to cause an inhomogeneous growth of the nanoparticles with relatively low concentration of Co^{2+} ions in the oxygen interstices. In addition, this faulty growth mechanism gave rise to an increase in the size of the produced nanocrystals. Omitting the polyol cosurfactant from the synthesis caused a substantial increase in the MO response, which together with the Raman spectroscopy data indicated an increased concentration of Co^{2+} incorporated in the lattice. It was possible to drive part of the cobalt ions from tetrahedral to octahedral sites using Zn^{2+} as a dopant or Co^{3+} precursor instead of Co^{2+}. This work demonstrates the importance of fine tuning a colloidal synthesis to obtain efficient doping in nanocrystals.

Acknowledgment. This work was supported by Israel Science Foundation Grant 779/06 and the James Frank program. The authors acknowledge useful discussions with Professor M. Kol.

References and Notes

(1) Telem-Shafir, T.; Markovich, G. *J. Chem. Phys.* **2005**, *123*, 204715.
(2) Maenosono, S.; Okubo, T.; Yamaguchi, Y. *J. Nanopart. Res.* **2003**, *5*, 5.
(3) Parker, A. J.; Childs, P. A.; Palmer, R. E. *Microelectron. Eng.* **2002**, *61*−*62*, 681.
(4) Tseng, R. J.; Ouyang, J.; Chu, C. W.; Huang, J. S.; Yang, Y. *Appl. Phys. Lett.* **2006**, *88*, 123506.
(5) Murray, P. J.; Linnett, J. W. *J. Phys. Chem. Solids* **1976**, *37*, 619.
(6) Yang, C. S.; Awshalom, D. D.; Stucky, G. D. *Chem. Mater*. **2001**, *13*, 594.
(7) Bai, F. F.; He, Y.; He, P.; Tang, Y. W.; Jia, Z. J. *Mater. Lett*. **2006**, *60*, 3126.
(8) Kahn, M. L.; Monge, M.; Colliere, V.; Senoq, F.; Maisonnat, A.; Chaudret, B. *Adv. Func. Mater*. **2005**, *15*, 458.
(9) Barker, A. J.; Cage, B.; Russek, S.; Stoldt, C. R. *J. Appl. Phys*. **2005**, *98*, 063528.
(10) Zhong, X.; Han, M.; Dong, Z.; White, T. J.; Knoll, W. *J. Am. Chem. Soc*. **2003**, *125*, 8589.
(11) Fitzgerald, C. B.; Venkatesan, M.; Lunney, J. G.; Dorneles, L. S.; Coey, J. M. D. *Appl. Surf. Sci.* **2005**, *247*, 493.
(12) Meron, T.; Markovich, G. *J. Phys. Chem. B* **2005**, *109*, 20232.
(13) Sun, S.; Murray, C. B.; Weller, D.; Folks, L.; Moser, A. *Science* **2000**, *287*, 1989.
(14) Dobrynin, A. N.; Ievlev, D. N.; Verschoren, G.; Swerts, J.; Van Bael, M. J.; Temst, K.; Lievens, P.; Piscopiello, E.; Van Tendeloo, G.; Zhou, S. Q.; Vantomme, A. *Phys. Rev. B* **2006**, *73*, 104421
(15) Shevchenko, E. V.; Talapin, D. V.; Schnablegger, H.; Kornowski, A.; Festin, O.; Svedlidh, P.; Hasse, M.; Weller, H. *J. Am. Chem. Soc*. **2003**, *125*, 9090.
(16) Tailhades, P.; Bonningue, C.; Rousset, A.; Bouet, L.; Pasquet, I.; Lebrun, S. *J. Magn. Magn. Mater*. **1999**, *193*, 148.
(17) Gu, B. X. *Appl. Phys. Lett.* **2003**, *82*, 3707.
(18) Peeters, W. L.; Martens, J. W. D. *J. Appl. Phys.* **1982**, *53*, 8178.
(19) Antonov, V. N.; Harmon, B. N.; Antropov, V. P.; Perlov, Y. A.; Yresko, A. N. *Phys. Rev. B* **2001**, *64*, 134410.
(20) Hyeon, T. *Chem. Commun.* **2003**, *8*, 927.
(21) Manova, E.; Kunev, B.; Paneva, D.; Mitov, I.; Petrov, L. *Chem. Mater*. **2004**, *16*, 5689.
(22) Fried, T.; Shemer, G.; Markovich, G. *Adv. Mater*. **2001**, *13*, 1158.
(23) Ferreira, T. A. S.; Waerenborgh, J. C.; Mendonca, M. H. R. M.; Costa, F. M. *Solid State Sci.* **2003**, *5*, 384.
(24) Pillali, V.; Shah, D. O. *J. Magn. Magn. Mater*. **1996**, *163*, 243.
(25) Rondinone, A. J.; Samia, A. C. S.; Zhang, Z. J. *J. Phys. Chem. B* **1999**, *103*, 6876.
(26) Meron, T.; Rosenberg, Y.; Lereah, Y.; Markovich, G. *J. Magn. Magn. Mater.* **2005**, *292*, 11.
(27) Bensebaa, F.; Zavaliche, F.; L'Ecuyer, P.; Cochrane, R. W.; Veres, T. *J. Colloid Interface Sci.* **2004**, *277*, 104.
(28) Tirosh, T.; Shemer, G.; Markovich, G. *Chem. Mater*. **2006**, *18*, 465.
(29) Sun, S.; Zeng, H.; Robinson, D. B; Raoux, S.; Rice, P. M.; Wang, S. X.; Li, G. *J. Am. Chem. Soc.* **2004**, *126*, 273.
(30) Sato, K. *Jpn. J. Appl. Phys.* **1981**, *20*, 2403.
(31) Krumme, J. P.; Doormann, V.; Klages, C. P. *Appl. Opt*. **1983**, *23*, 1184.
(32) Fontijn, W. F. J.; van der Zaag, P. J.; Feiner, L. F.; Metselaar, R.; Devillers, M. A. C. *J. Appl. Phys.* **1999**, *85*, 5100.
(33) de Faraia, D. L. A; Venancio Silva, S., de Oliviera, M. T. J. R *J. Raman Spectrosc.* **1997**, *28*, 873.
(34) Kip, B. J.; Meier, R. J. *Appl. Spectroc*. **1990**, *44*, 707.
(35) Song, Q.; Zhang, Z. J. *J. Am. Chem. Soc.* **2004**, *126*, 6164.
(36) Niederberger, M.; Garnweitner, G. *Chem.*−*Eur. J* **2006**, *12*, 7282.
(37) Chinnamasy, C. N.; Jeyadevan, B.; Shinoda, K.; Tohji, K. *J Appl. Phys.* **2003**, *93*, 7583.
(38) Wan, S. R.; Zheng, Y.; Liu, Y. Q.; Yan, H. S.; Liu, K. L. *J. Mater. Chem.* **2005**, *15*, 3424.
(39) Suzuki, K.; Namilawa, T.; Yamazaki, Y. *Jpn. J Appl. Phys.* **1988**, *27*, 361.
(40) Lide, D. R. *Handbook of Chemistry and Physics*, 72nd ed.; CRC Press: Boca Raton, FL, 1991.
(41) Hochepied, J. F.; Pileni, M. P. *J. Appl. Phys.* **2000**, *87*, 2472.
(42) See, for example, the spectra in the following papers: (a) da Silva, S. W.; Melo, T. F. O.; Soler, M. A. G.; Lima, E. C. D.; da Silva, M. F.; Morais, P. C. *IEEE Trans. Magn*. **2003**, *39*, 2645. (b) Viart, N.; Rebmann, G.; Pourroy, G.; Loison, J. L.; Versini, G.; Huber, F.; Ulhaq-Bouillet, C.; Me'ny, C.; Panissod, P.; Saviot, L. *Thin Solid Films* **2005**, *471*, 40. (c) Yu, T.; Shen, Z. X.; Shi, Y.; Ding, J. *J. Phys.: Condens. Matter* **2002**, *14*, L613. (d) Wang, W. H.; Ren, X. *J. Crystal Growth* **2006**, *289*, 605.
(43) Wang, Z.; Downs, R. T.; Pischedda, V.; Shetty, R.; Saxena, S. K.; Zha, C. S.; Zhao, Y. S.; Schiferl, D.; Waskowska, A. *Phys. Rev. B* **2003**, *68*, 094101.
(44) Yu, T.; Shen, Z. X.; Shi, Y.; Ding, J. *J. Phys.: Condens Matter* **2002**, *14*, L613.
(45) Chamritski, I.; Burns, G. *J. Phys. Chem. B* **2005**, *109*, 4965.
(46) Gasparov, L. V.; Tanner, D. B.; Romero, D. B; Berger, H.; Margaritondo, G.; Forro, L. *Phys. Rev. B* **2000**, *62*, 7939.